Involvement of PHOSPHATE TRANSPORTER TRAFFIC FACILITATOR1 in COPII assembly by interacting with SAR1 GTPase

Hui-Fang Lung (龍惠方)[a], Jia-Dong Chu[a], Tzu-Yin Liu[a, b,1]

[a]Institute of Bioinformatics and Structural Biology, College of Life Sciences and Medicine, National Tsing Hua University, Hsinchu 30013, Taiwan.

[b]Department of Life Science, College of Life Sciences and Medicine, National Tsing Hua University, Hsinchu 30013, Taiwan.

[1]Address correspondence to tzliu@life.nthu.edu.tw

Institute of Bioinformatics and Structural Biology, College of Life Sciences and Medicine, National Tsing Hua University, Hsinchu 30013, Taiwan

Tel: +886 3 574-2096, Fax: +886 3 571-5934

The author responsible for distribution of materials integral to the findings presented in this article in accordance with the policy described in the Instructions for Authors (https://academic.oup.com/plphys/pages/General-Instructions) is: Tzu-Yin Liu (tzliu@life.nthu.edu.tw).

Running title: PHF1 interacts with SAR1 GTPase

Abstract

The plant-specific endoplasmic reticulum (ER)-resident PHOSPHATE TRANSPORTER TRAFFIC FACILITATOR1 (PHF1) is structurally related to SEC12, which initiates the coat protein complex II (COPII) assembly as a guanine nucleotide exchange factor (GEF) by activating the small GTPase SAR1. In contrast, PHF1 loses the conserved catalytic residues critical for GEF activity and instead specifically assists the ER exit of the plant PHOSPHATE TRANSPORTER1 (PHT1) family. However, the underlying molecular mechanism remains to be elucidated. In this study, we showed that the overexpression of *Arabidopsis thaliana* PHT1;1 (*At*PHT1;1) but not of SUGAR TRANSPORTER 1 (*At*STP1) caused a portion of *At*PHF1 distribution into *At*SAR1b-, *At*SAR1c- and *At*SEC24a-labeled ER exit sites in the tobacco transient expression system. Based on the *in-planta* tripartite split-GFP association, *At*PHF1 interacted with *At*SAR1b and *At*SAR1c but not with other COPII-related proteins. By performing the miniTurbo-based proximity labeling in agro-infiltrated tobacco leaves, we verified the interaction of *At*PHF1 and *At*SAR1b and demonstrated its physiological relevance by co-immunoprecipitation of the endogenous *At*PHF1 and *At*PHT1;1/2/3 proteins with *At*SAR1c-GFP using *Arabidopsis* transgenic lines. Furthermore, while both the cytosolic and transmembrane domains of *At*PHF1 contribute to the interaction with *At*SAR1b and *At*SAR1c, *At*PHF1 preferentially interacted with the GDP-locked inactive form of *At*SAR1b. On the basis of these findings, we propose that by interacting with SAR1 GTPase, PHF1 participates in the early step of COPII recruitment for the ER export of PHT1 proteins.

Keywords: coat protein complex II (COPII), PHOSPHATE TRANSPORTER TRAFFIC FACILITATOR1, ER export, PHOSPHATE TRANSPORTER1

Introduction

As sessile organisms, plants adjust the protein and lipid composition of the plasma membrane (PM) to sense and adapt to the ever-changing environment. Such dynamic cellular processes heavily rely on the modulation of the endomembrane trafficking system (Wang et al., 2020), including the coat protein complex II (COPII)-mediated endoplasmic reticulum (ER)-to-Golgi transport pathway. Although the core COPII machinery composed of five cytosolic factors, SAR1, SEC23, SEC24, SEC13, and SEC31, is conserved throughout all eukaryotes, the mechanisms underlying COPII recruitment and assembly are most extensively studied in the budding yeast *Saccharomyces cerevisiae* (Barlowe and Miller, 2013). In this model organism, the COPII-related components are encoded by single genes and recruited sequentially to the ER exit sites (ERES) (Kurokawa and Nakano, 2019). The SAR1 GTPase is activated upon the exchange of GDP to GTP by the guanine nucleotide exchange factor (GEF) SEC12, exposing its amphipathic N-terminal helix to be inserted into the ER membrane (d'Enfert, 1991; Paul et al., 2023). SAR1 then interacts directly with SEC23, inducing the formation of the inner coat SEC23–SEC24 complex, which in turn recruits the outer coat SEC13–SEC31 complex (Bi, 2002; Stagg et al., 2006). In addition, SEC16, an initial factor assembled at the ERES, serves as a scaffold protein by concentrating SEC12 and GTP-bound active SAR1 in proximity (Supek et al., 2002; Connerly et al., 2005). By comparison, the plant COPII subunit paralogs are encoded by multi-gene families and outnumber those in other organisms (Chung et al., 2016). Multiple COPII paralogues allow the diversity of COPII transport carriers to adapt to various developmental and stress-related cues (Wang et al., 2020; Li et al., 2022). For instance, the phytohormone abscisic acid triggered the formation of *Arabidopsis thaliana* SAR1a (*At*SAR1a)-dependent COPII vesicles that carry osmotic stress-related carriers (Li, 2021). The *At*SAR1a-*At*SEC23a pairing was also shown to mediate the ER export of the ER-associated transcription factor bZIP28, which is upregulated under ER stress (Zeng et al., 2015). By

contrast, how the COPII machinery regulates protein ER export to cope with nutrient deficiency remains unknown.

Inorganic phosphate (Pi) is an essential macronutrient for plant growth. Due to its poor solubility and mobility in soil, Pi bioavailability is limited, thus causing plants to face Pi deficiency (Shen, 2011). Under Pi-limited conditions, plants enhance the external Pi uptake as well as the recycling and remobilization of internal Pi, which involves the upregulation of the *PHOSPHATE TRANSPORTER1* (*PHT1*) gene family at the transcript and post-transcriptional level (Nussaume et al., 2011). While most *PHT1* genes are upregulated by Pi deprivation, the newly synthesized PHT1 proteins (PHT1s) must exit the ER for the PM targeting. Similar to the inhibitory effect of SEC12 overexpression on the ER export of the Golgi transmembrane protein ERD2 in tobacco leaves (Hanton et al., 2007), the overexpression of SEC12 impaired the PM targeting of the *Arabidopsis thaliana* PHT1;2 (*At*PHT1;2) (Bayle et al., 2011). Thus, the ER-to-Golgi transport of PHT1s is dependent on efficient COPII assembly. Interestingly, the plant-specific SEC12-related protein PHOSPHATE TRANSPORTER TRAFFIC FACILITATOR1 (PHF1) was identified to facilitate the ER exit of *At*PHT1s (Gonzalez et al., 2005; Bayle et al., 2011). Despite sharing the sequence similarity with SEC12, *At*PHF1 lost the conserved catalytic residues critical for GEF activity and failed to rescue the growth defect of the yeast *sec12* mutant (Gonzalez et al., 2005). Instead, the *Arabidopsis* loss-of-function *phf1* mutant showed decreased cellular Pi content and impaired PM targeting of *At*PHT1;1 (Gonzalez et al., 2005). As the role of PHF1 in assisting the ER exit of PHT1s resembles that of the yeast Pho86p in the ER exit of Pho84p, the yeast homolog of PHT1s (Lau, 2000), PHF1 may functionally diverge from SEC12 (Gonzalez et al., 2005).

The transient protein expression using tobacco leaves is a well-established plant system to study the dynamic organization of COPII proteins at the ERES (daSilva et al., 2004; Hanton et al., 2009). In this system, the ERES formation can be monitored by the subcellular distribution of fluorescent protein-tagged COPII components changing from cytosolic patterns into punctate

structures (daSilva et al., 2004; Hanton et al., 2007; Hanton et al., 2008; Hanton et al., 2009). Overexpression of COPII-dependent membrane cargoes enhanced the recruitment of YFP-*At*SEC24a to the ERES and induced the *de novo* formation of ERES (Hanton et al., 2007). Likewise, *At*PHT1;2-CFP overexpression resulted in the recruitment of YFP-*At*SEC24a and YFP-*Sc*Sar1 to the ERES puncta (Bayle et al., 2011). Although the co-expression study showed that the ER-resident *At*PHF1 failed to co-localize with *At*SEC24a, thus leading to the conclusion that *At*PHF1 is not involved in COPII recruitment (Bayle et al., 2011), it is unclear whether PHF1 participates in cargo recognition and selective packaging of PHT1 Pi transporters into COPII vesicles.

Since PHF1 shares sequence similarity with SEC12 yet exhibits a distinct function, we speculated that PHF1 may engage the COPII-dependent ER export of PHT1s on a molecular basis different from SEC12. To explore this hypothesis, we aimed to investigate whether *At*PHT1;1 overexpression can induce the distribution of *At*PHF1 into ERES puncta and whether *At*PHF1 can interact with COPII-related components. Using agro-infiltrated tobacco leaves, we showed that overexpression of *At*PHT1;1 triggered a portion of *At*PHF1 distribution into punctate structures that partially co-localized with *At*SAR1b, *At*SAR1c and *At*SEC24a. Furthermore, *At*PHF1 interacted with *At*SAR1b and *At*SAR1c but not with *At*SEC24a and other COPII-related components based on tripartite split-GFP association. Consistently, we verified the interaction of *At*PHF1 and *At*SAR1b by the proximity labeling in the transient tobacco system and demonstrated that the endogenous *At*PHF1 and *At*PHT1;1/2/3 was co-immunoprecipitated with the *At*SAR1c-GFP in the *Arabidopsis* transgenic line. More importantly, we showed that like *At*SEC12, *At*PHF1 preferentially interacted with the GDP-locked inactive form of *At*SAR1b. Our results unveiled that *At*PHF1 acts as an early regulator of COPII assembly for the ER export of PHT1s through interacting with *At*SAR1 proteins (*At*SAR1s).

Results

Overexpression of *At*PHT1;1 triggers the partial distribution of *At*PHF1 into ERES-associated punctate structures

Both the mammalian and plant SEC12 proteins are dispersed throughout the ER (Weissman et al., 2001; Bayle et al., 2011). However, the mammalian SEC12 can be concentrated at the ERES by the collagen cargo receptor component cTAGE5 for the ER export of collagen (Saito et al., 2014). We thus wondered whether *At*PHF1, which distributes evenly across the ER (Gonzalez et al., 2005; Bayle et al., 2011), can be induced to concentrate at the ERES when the ER export of *At*PHT1;1 is highly demanded. When expressed alone in agro-infiltrated tobacco leaves, *At*PHF1-GFP showed a reticular ER pattern, while a portion of *At*PHF1-GFP showed punctate-like structures when the split-GFP tagged *At*PHT1;1 (*At*PHT1;1-S11) was co-expressed (**Fig. 1A**). By contrast, the co-expression of *At*PHF1-GFP with the sugar transporter *At*STP1-S11 did not change the distribution of *At*PHF1-GFP (**Fig. 1A**). Statistical analysis further suggested that the overexpression of *At*PHT1;1-S11 but not of *At*STP1-S11 significantly triggered the partial distribution of *At*PHF1-GFP into punctate structures (**Fig. 1B**).

In the tobacco transient expression system, the co-expression of membrane cargoes recruited the COPII components, such as *At*SAR1s and *At*SEC24, to concentrate at the punctate ERES (Hanton et al., 2007; Hanton et al., 2008). To address whether the punctate structures of *At*PHF1-GFP induced by the overexpression of *At*PHT1;1 might represent ERES, we selected *At*SAR1b as the COPII marker to co-localize with *At*PHF1-mCherry. This is because *AtSAR1b* is the most highly expressed *AtSAR1* gene in roots and is upregulated by Pi deprivation (Liu et al., 2016) (**Supplementary Fig. S1**). In addition, the previous proteomic analysis of the Pi overaccumulator *pho2* root has revealed the co-induction of *At*SAR1b and *At*PHT1s (Huang et al., 2013), implying an increased demand for *At*SAR1b to promote the ER-to-Golgi traffic of *At*PHT1s. Considering that the N-terminal tail of SAR1 is inserted into the ER membranes upon

activation (d'Enfert, 1991; Paul et al., 2023), we fused the S11 tag to the C terminus of *At*SAR1b to prevent steric hindrance. In tobacco epidermal cells, *At*SAR1b-S11 exhibited both a diffuse cytosolic distribution and an ER membrane-associated punctate pattern (**Supplementary Fig. S2A**). As *AtSAR1c* is the second most expressed *AtSAR1* gene in roots (Liu et al., 2016) (**Supplementary Fig. S1**) and plays an interchangeable role with *AtSAR1b* in pollen development at the protein level (Liang et al., 2020), we also included *At*SAR1c-S11 for comparison. *At*SEC24a is involved in the cargo selection for COPII vesicles and is also widely used as a reliable ERES marker (Miller, 2002; Hanton et al., 2007), so we generated the construct expressing *At*SEC24a-S11 for co-localization with *At*PHF1-GFP as well. The subcellular localizations of *At*SAR1b-S11 and *At*SAR1c-S11, as detected by the complementation of GFP1–10, were similar to the previously reported results (Hanton et al., 2008; Zeng et al., 2015) (**Supplementary Fig. S2A**). *At*SEC24a-S11 also displayed the cytosolic and punctate patterns (**Supplementary Fig. S2A**). While the co-expression of *At*PHF1-mCherry did not affect the subcellular distribution of *At*SAR1b and *At*SEC24a, the *At*PHT1;1 overexpression-induced punctate structures of *At*PHF1-mCherry co-localized with *At*SAR1b- and *At*SEC24a-labeled ERES (**Fig. 2A** and **2B**). Pearson's correlation analysis further revealed that *At*PHF1-mCherry puncta co-localized better with *At*SAR1b than with *At*SEC24a, as indicated by a statistically significant higher coefficient for *At*SAR1b (**Fig. 2C**). Similarly, *At*PHF1-mCherry puncta partially co-localized with *At*SAR1c (**Supplementary Fig. S2B**). There was no significant difference in the co-localization coefficient between *At*SAR1b and *At*SAR1c (**Supplementary Fig. S2C**). Taken together, these results suggested that when *At*PHT1;1 is overexpressed as the COPII-dependent export membrane cargo, *At*PHF1 can partially distribute into the puncta associated with the ERES markers.

The interaction of *At*PHF1 with *At*SAR1b/c *in planta* based on tripartite split-GFP association

As *At*PHT1;1 overexpression triggered the distribution of *At*PHF1 partially into punctate structures that are associated with *At*SAR1b, *At*SAR1c and *At*SEC24a, we postulated that *At*PHF1 may participate in the COPII recruitment or assembly. To explore this possibility, we examined the interaction of *At*PHF1 with several COPII-related components using the tripartite split-GFP assay in agro-infiltrated tobacco leaves (Cabantous et al., 2013; Liu et al., 2018). The expression of split-GFP tagged *At*SEC12 and *At*PHF1 (S10-*At*SEC12 and S10-*At*PHF1) confirmed their localization at the ER when co-expressed with the cytosolic S11-GFP1–9 (**Fig. 3A**). We also generated the constructs expressing the split-GFP tagged *At*SEC16a and *At*SEC13a (*At*SEC16a-S11 and *At*SEC13a-S11). As previously reported (Hanton et al., 2009; Takagi et al., 2013), *At*SEC16a-S11 predominantly localized to the cytosol, while *At*SEC13a-S11 displayed both the cytosol and nucleus patterns (**Fig. 3A**). As expected, S10-*At*SEC12 as a positive control for the protein-protein interaction interacted with *At*SAR1b and *At*SAR1c, yielding the GFP complementation signals (**Fig. 3B**). Notably, like S10-*At*SEC12, S10-*At*PHF1 interacted with *At*SAR1b-S11 but not with *At*SEC24a-, *At*SEC16a-, and *At*SEC13a-S11 (**Fig. 3B**). A similar interaction pattern was also observed for *At*PHF1 with *At*SAR1c (**Fig. 3B**), reinforcing the specificity of *At*PHF1 interaction with *At*SAR1s.

The interaction of *At*PHF1 with *At*SAR1b *in planta* based on miniTurbo (mTb) proximity labeling

Although the tripartite split-GFP association detects protein-protein interaction without spurious background signals (Cabantous et al., 2013; Liu et al., 2018), the reconstitution of split-GFP fragments may result from a non-specific irreversible interaction. Therefore, we used the proximity labeling method as a complementary approach to validate the interaction of *At*PHF1 and *At*SAR1b *in planta*. Proximity labeling starts after the application of biotin and can be reversibly halted by removing biotin, thus allowing the capture of transient and dynamic protein-protein interaction at a ten-nanometer scale (Xu et al., 2023). Due to the superior

feasibility of miniTurbo (mTb) in the tobacco system (Mair et al., 2019), the mTb-based proximity labeling was used to assess whether *At*PHF1 is in close proximity to *At*SAR1b. For unknown reasons, our initial attempt to express mTb-EYFP-*At*PHF1 in agro-infiltrated tobacco leaves was unsuccessful, so we generated the *At*SAR1b-mTb-S11 construct by fusing mTb to *At*SAR1b (**Fig. 4A**). We also used the cytosol-localized mTb-NES-EYFP, which carries the nuclear export sequence (NES), as a negative control (Mair et al., 2019). Taking the advantage that S11 can self-complement with GFP1–10, we could detect the expression and subcellular distribution of *At*SAR1b-mTb-S11 in agro-infiltrated tobacco leaves (**Fig. 4B**). We then co-expressed mTb-NES-EYFP or *At*SAR1b-mTb-S11 with *At*SEC12-mCherry or *At*PHF1-mCherry and incubated the harvested leaves in a biotin solution, followed by tissue homogenization and protein extraction. The protein extraction of non-infiltrated tobacco leaves was used for the background comparison (**Fig. 4C**). As the expression of the cytosolic mTb-NES-EYFP was much greater than the membrane-associated *At*SAR1b-mTb-S11, we adjusted the ratio of protein amount for *At*SAR1b-mTb-S11: mTb-NES-EYFP to 30: 1. In such a way, the protein amounts of mTb-NES-EYFP and *At*SAR1b-mTb-S11 were comparable to fairly compete with binding to streptavidin beads. When co-expressed with *At*SAR1b-mTb-S11, *At*SEC12-mCherry and *At*PHF1-mCherry could be immunoprecipitated by streptavidin and detected by immunoblot, indicating that they were biotinylated (**Fig. 4C**). By contrast, the co-expression of mTb-NES-EYFP with *At*SEC12-mCherry or *At*PHF1-mCherry did not yield similar effects (**Fig. 4C**). These results again suggested that *At*PHF1 interacts with *At*SAR1s *in planta*.

Co-immunoprecipitation of the endogenous *At*PHF1 with *At*SAR1c-GFP in *Arabidopsis* root

To answer whether the interaction of *At*PHF1 and *At*SAR1s is physiologically relevant, we used the *Arabidopsis* transgenic plants expressing *At*SAR1c-GFP or GFP under the UBQ10

promoter for co-immunoprecipitation (co-IP) (Zeng et al., 2015). The *Arabidopsis* seedlings were subjected to seven days of Pi starvation to mimic the physiological conditions in which the endogenous *At*PHF1 is upregulated and the ER export of *At*PHT1 proteins is also highly demanded. Total root protein extract was immunoprecipitated with GFP-Trap beads followed by immunoblot using an anti-*At*PHF1 specific antibody. Due to the differences in the expression level between the cytosolic GFP and the membrane-associated *At*SAR1c-GFP in transgenic plants, we increased the protein amount for the co-IP of *At*SAR1c-GFP by 50-fold than that for the co-IP of GFP (**Fig. 5A**). Immunoblot of the IP suggested that the endogenous *At*PHF1 was co-immunoprecipitated with *At*SAR1c-GFP but not with GFP (**Fig. 5A**). Conversely, when we used equal amounts of root total protein for the co-IP experiments, the *At*SAR1c-GFP expression was ten times lower than the GFP expression but co-immunoprecipitated more endogenous *At*PHF1 (about 3.1-fold) (**Fig. 5B**), suggesting that *At*SAR1c-GFP exhibits a higher binding affinity toward *At*PHF1. Moreover, the endogenous *At*PHT1;1/2/3 proteins could also be co-immunoprecipitated with *At*SAR1c-GFP (**Fig. 5A and 5B**), indicating that the presence of protein complex containing *At*SAR1s, *At*PHF1 and *At*PHT1s. These data supported the notion that by interacting with *At*SAR1s, *At*PHF1 participates in the initial phase of COPII assembly for the ER export of *At*PHT1s.

The cytosolic and transmembrane domains of *At*PHF1 interact with *At*SAR1b and *At*SAR1c

To determine which region of *At*PHF1 is involved in the interaction with *At*SAR1s *in planta*, we generated four N-terminally S10-tagged *At*PHF1 truncated variants as follows: the cytoplasmic domain alone (*At*PHF1 N), the cytoplasmic domain with the transmembrane (TM) domain (*At*PHF1 N–TM), the TM domain alone (*At*PHF1 TM), and the TM domain with the ER-luminal domain (*At*PHF1 TM–C) (**Fig. 6A**). The expression and the subcellular distribution of these *At*PHF1 variants suggested that S10-*At*PHF1 N was present in the cytosol and nucleus,

while the other truncated forms of *At*PHF1 localized to the ER (**Supplementary Fig. S3A**). The subcellular localization of the C-terminally S11-tagged truncated forms of *At*PHF1 also showed similar results (**Supplementary Fig. S3B**), suggesting that the TM domain of *At*PHF1 alone is sufficient for its ER targeting. As all the S10-tagged truncated *At*PHF1 variants interacted with *At*SAR1b-S11 (**Fig. 6B**) and *At*SAR1c-S11 (**Fig. 6C**), we concluded that both the cytosolic and the TM domains of *At*PHF1 contribute to the interaction with *At*SAR1.

*At*PHF1 preferentially interacts with the GDP-locked inactive form of *At*SAR1b

Because the assembly and disassembly of COPII is controlled by the Sar1 GTPase cycle (Van der Verren and Zanetti, 2023), we next asked whether *At*PHF1 interacts with *At*SAR1s in a specific nucleotide-binding state. The wild-type *At*SAR1b-S11 and the GTP-locked *At*SAR1b[H74L]-S11 localized to both the ER membrane and cytosol as previously reported (daSilva et al., 2004; Wei and Wang, 2008) (**Fig. 7A**). The GDP-locked *At*SAR1b[T34N]-S11 also displayed a similar subcellular pattern (**Fig. 7A**). However, based on the biochemical fractionation that distinguishes the soluble and microsomal fractions, the membrane-associated proportion of the wild-type *At*SAR1b-S11, the *At*SAR1b[H74L]-S11 and the *At*SAR1b[T34N]-S11 were 64%, 63%, and 51%, respectively, indicating that the GDP-locked form of *At*SAR1b was less membrane-associated (**Supplementary Fig. S4**). These results were in agreement with the finding that upon the binding of GTP, SAR1 is activated to being inserted into the ER membrane (d'Enfert, 1991; Paul et al., 2023). More importantly, the *in-planta* tripartite split-GFP assay suggested that *At*PHF1 interacted with the GDP-locked form of *At*SAR1b but not with the GTP-locked form of *At*SAR1b (**Fig. 7B**), indicating that, like SEC12, PHF1 preferentially interacts with the GDP-bound SAR1 and thus may be involved in recruiting COPII components to the ER membranes.

Discussion

Although several ER accessory proteins have been identified to participate in the ER exit of membrane proteins, the underlying molecular mechanisms are mostly unclear (Lau, 2000; Kota and Ljungdahl, 2005). In *Arabidopsis*, AUXIN RESISTANCE4 (AXR4) was shown to interact with auxin influx carriers AUX1 and LAX2 to promote their PM targeting (Dharmasiri, 2006; Tidy et al., 2024). The KAONASHI3 (KNS3) family is recently identified to mediate the ER exit of the boric acid channel *At*NIP5;1 (Zhang et al., 2024). While *At*PHF1 is required for the PM targeting of *At*PHT1s, it was proposed to act as an ER-localized chaperone for the protein stability of *At*PHT1s (Gonzalez et al., 2005) and not participate in the COPII vesicle formation (Bayle et al., 2011). On the contrary, our data revealed a role for *At*PHF1 in the early step of COPII assembly through the interaction with *At*SAR1s. Using the three different methods, i.e., tripartite split-GFP complementation, proximity labeling, and co-immunoprecipitation, we showed that *At*PHF1 interacted with *At*SAR1s *in planta*. Furthermore, the *in-planta* tripartite split-GFP assay demonstrated that *At*PHF1 preferentially interacted with the GDP-bound *At*SAR1s. Our findings uncover that *At*PHF1 likely mediates the assembly of COPII vesicles by interacting with *At*SAR1s, thus facilitating the ER export of *At*PHT1s (**Fig. 8**).

The COPII recruitment to ERES is increased in response to the demand for ER export of membrane cargoes (Hanton et al., 2007). Our results showed that the transient overexpression of *At*PHT1;1 in *N. benthamiana* leaves also triggered partial distribution of *At*PHF1 into the punctate structures associated with the ERES markers *At*SAR1b, *At*SAR1c and *At*SEC24a (**Fig. 1, Fig. 2**, and **Supplementary Fig. S2**). In other words, under increased demand for the COPII-mediated export of *At*PHT1s, *At*PHF1 may partially relocate to the ERES to promote this process. Although *At*PHF1 lacks the conserved residues required for GEF activity and cannot complement the yeast *sec12* growth defect (Gonzalez et al., 2005), we surmised that upon *At*PHT1;1 overexpression, the distribution of *At*PHF1 to the ERES may facilitate the COPII recruitment or assembly. We reasoned that without high expression of *At*PHT1s, observing

partial co-localization of *At*PHF1 with ERES is beyond the detection limit of confocal imaging, which may explain the discrepancy between the results from a previous study (Bayle et al., 2011) and ours. In support of this notion, we showed that in transgenic plants subjected to Pi starvation, the endogenous *At*PHF1 and *At*PHT1;1/2/3 were co-immunoprecipitated with *At*SAR1c-GFP (**Fig. 5**), suggesting that the interaction of *At*PHF1 and *At*SAR1s is physiologically relevant. In addition, *At*PHF1 interacted with *At*SAR1b and *At*SAR1c but not with other COPII-related components (**Fig. 3B**), indicating that *At*PHF1 participates in the early step of COPII assembly, thus likely assisting the loading of *At*PHT1s into COPII vesicles for the ER export. Furthermore, we demonstrated that *At*PHF1 preferentially interacted with the GDP-locked form of *At*SAR1b *in planta* (**Fig. 7B**). These results indicated that *At*PHF1 could link the specific recognition of *At*PHT1s with the modulation of *At*SAR1s activity for the COPII assembly. Such a mechanism is dissimilar to that reported for SED4, the yeast structural homolog of SEC12 lacking GEF activity (Gimeno, 1995; Kodera et al., 2011). Genetic and biochemical evidence suggested that SED4 and SEC12 are not functionally interchangeable and that SED4 weakly inhibits the GTPase-activating (GAP) activity of SEC23 toward SAR1 (Saito-Nakano and Nakano, 2000). On the contrary, an *in vitro* study showed that SED4 had stronger binding to the non-hydrolyzable GTP analog GMPPNP-bound SAR1 and stimulated SEC23 GAP activity, thereby accelerating the dissociation of COPII coats from the ER membrane (Gimeno, 1995; Kodera et al., 2011). Unlike the interaction of SED4 and SEC16 required for the localization of SEC16 to ERES (Gimeno, 1995), the interaction of *At*PHF1 and *At*SEC16a was not observed (**Fig. 3B**). As many COPII-related factors regulate SAR1 activity through direct or indirect interaction (Van der Verren and Zanetti, 2023), we propose that *At*PHF1 modulates the recruitment efficiency of *At*SAR1s, thereby facilitating the formation of COPII vesicles carrying *At*PHT1s (**Fig. 8**).

*At*PHF1 is an ER-resident membrane protein not incorporated into COPII vesicles (Bayle et al., 2011). Interestingly, we recently reported that the *Arabidopsis* CORNICHON

HOMOLOG 5 (*At*CNIH5) acts as an ER cargo receptor that cycles between the ER and the early Golgi and selects *At*PHT1s for ER export (Chiu et al., 2024; Liu et al., 2024). *At*CNIH5 is preferentially expressed in the outer layers of the root above the apical meristem and interacts with *At*PHF1 (Chiu et al., 2024). As *At*PHF1 increased in the root of *cnih5* and the *cnih5 phf1* mutant showed more severe growth defects than the *phf1* single mutant (Chiu et al., 2024), we suspected that *At*PHF1 and *At*CNIH5 work interdependently. Namely, *At*PHF1 couples the recruitment of COPII proteins and *At*PHT1s by simultaneously interacting with *At*PHT1s and *At*SAR1s, while *At*CNIH5 is involved in the selective packaging of *At*PHT1 into COPII by interacting with other COPII components.

*At*PHF1 is structurally related to SEC12 proteins, which adopt a seven-bladed β propeller (Gonzalez et al., 2005; Joiner and Fromme, 2021). Based on the crystal structure, the catalytically critical K loop within the cytoplasmic domain of yeast SEC12 makes direct contact with nucleotide-free SAR1 (McMahon et al., 2012; Joiner and Fromme, 2021). Our data showed that both the cytosolic and the transmembrane domains of *At*PHF1 interact with *At*SAR1b/c *in planta* (**Fig. 6**), indicating that the interaction interface may reside across relatively large areas. Since the catalytic residues required for GEF activity are absent in *At*PHF1 (Gonzalez et al., 2005), it awaits to elucidate whether the interaction interface of PHF1-SAR1s is different from that of SEC12-SAR1s and how PHF1 modulates the recruitment of SAR1s without GEF activity.

Materials and Methods

Plant material and growth conditions

The seeds of *Arabidopsis thaliana* wild-type (WT) (Columbia, Col-0) and *phf1* were obtained from the Arabidopsis Biological Resource Center (ABRC). Seeds of *A. thaliana* were surface-sterilized and germinated on one-half modified Hoagland agar plates, comprising 2.5 mM $Ca(NO_3)_2$, 2.5 mM KNO_3, 1 mM $MgSO_4$, 50 μM [NaFe(III) EDTA], 250 μM KH_2PO_4, 10 μM

H_3BO_3, 0.2 μM Na_2MoO_4, 1 μM $ZnSO_4$, 2 μM $MnCl_2$, 0.5 μM $CuSO_4$, 0.2 μM $CoCl_2$, 0.5 mM MES (pH 5.7), 1% Sucrose and 1% Bacto agar and grown in the growth chamber at 22℃ under a 16-h-light/8-h-dark cycle. The Pi-sufficient (+P) and Pi-deficient (−P) media were one-half modified Hoagland nutrient solutions containing 250 μM and 0 μM KH_2PO_4, respectively. Seeds of *Nicotiana benthamiana* (*N. benthamiana*) were surface-sterilized and germinated on Murashige and Skoog medium diluted 2-fold agar plates and grown in the growth chamber at 24℃ under a 16-h-light/8-h-dark cycle.

Plasmid construction

For the self-complementing split-GFP assay (Liu et al., 2018), the constructs encoding *UBQ10:sXVE:*GFP1–10 (Addgene plasmid #125663), *UBQ10:sXVE:*ER-GFP1–10 (Addgene plasmid #125664), *UBQ10:sXVE:*S11-GFP1–9 (Addgene plasmid #125665), or *UBQ10:sXVE:*ER-S11-GFP1–9 (Addgene plasmid #125666) was used. For the tripartite split-GFP association, the constructs encoding *UBQ10:sXVE:*GFP1–9 (Addgene plasmid #108187), *UBQ10:sXVE:*ER-GFP1–9, or *35S:*GFP1–9.pMDC201 was used. For constructing the S10-tagged clones, the CDS of *At*PHF1 and *At*SEC12 were amplified by PCR and subcloned into *UBQ10:sXVE:*S10-(MCS) (Addgene plasmid #108177). For constructing the S11-tagged clones, the CDS of *At*STP1 was amplified by PCR and subcloned into *UBQ10:sXVE:*(MCS)-S11 (Addgene plasmid #108179). The CDS of *At*PHT1;1 was amplified by PCR and subcloned into *UBQ10:sXVE:*(MCS)-3xHA-S11 (Addgene plasmid #108180). The CDS of *At*SAR1b, *At*SAR1b[H74L], *At*SAR1b[T34N], *At*SAR1c, *At*SEC24a, *At*SEC13a, and *At*SEC16a were amplified and subcloned into *UBQ10:*(MCS)-S11. For constructing the GFP fusion clones, the CDS of *At*PHF1 was amplified and subcloned into *UBQ10:*(MCS)-GFP. For constructing the mTb-fused clones, the CDS of mTb was amplified by PCR using R4pGWB601_UBQ10p-miniTurbo-NES-YFP (Addgene plasmid #127369) as the template and subcloned into *UBQ10:At*SAR1b-S11, yielding *UBQ10:At*SAR1b-mTb-S11. The abovementioned constructs

were generated either by restriction enzyme cloning or by In-Fusion® HD cloning (Takara). Primer sequences and the restriction enzyme cutting sites used are listed in **Supplementary Table S1**.

Agro-infiltration of *Nicotiana benthamiana* leaves

Three- to four-week-old of *Nicotiana benthamiana* plants were used for *A. tumefaciens* (strain EHA105)-mediated infiltration. The bacterial cultures were grown overnight in Luria-Bertani (LB) medium containing appropriate antibiotics (50 μg/ml spectinomycin, 5 μg/ml rifampicin, or 50 μg/ml kanamycin) at 30℃ with shaking at 200 rpm. After centrifugation, the pellet was resuspended in infiltration buffer containing 10 mM $MgCl_2$, 10 mM MES (pH 7.5), 150 μM acetosyringone to an OD_{600} of 1.0 and incubated at room temperature (RT) for 2–4 h. Tobacco leaves were infiltrated with the agrobacterial suspension at a final OD_{600} in the range of 0.01–1.0. For gene expression under the *UBQ10:sXVE* inducible promoter, the 9.18 μM ß-estradiol was applied for additional 24 or 48 h. The *N. benthamiana* leaves at 48 or 72 h post-infiltration were collected for confocal analysis or protein extraction.

Confocal image analysis

Confocal images were captured using the Zeiss LSM 800 microscope (Zeiss) equipped with Plan-Apochromat 10×/0.45 M27, 20×/0.8 M27, and 40×/1.3 Oil DIC M27 objectives. The acquisition was performed in multi-track mode with line switching, and the data were averaged over two readings. Excitation/emission wavelengths were 488 nm/410–546 nm, 561 nm/560–617 nm, and 488 nm/656–700 nm for GFP, mCherry, and chlorophyll autofluorescence, respectively. For the quantitative analysis of punctate structures in the epidermal cells of agro-infiltrated *N. benthamiana* leaves, the punctate structures were defined using the ImageJ (Schneider et al., 2012) ‘analyze particles’ function, and the Pearson’s correlation coefficient

was measured using the Fiji 'co-localization' function. The box plots were generated by using the BoxPlotR (Spitzer et al., 2014).

Proximity labeling assay

The *N. benthamiana* leaf tissues were incubated in 50 µM biotin solution (in DMSO) at RT for 30 min and ground with liquid N. The tissue powder was resuspended with two volumes (2 ml per gram tissue) of lysis buffer containing 20 mM HEPES (pH 7.5), 40 mM KCl, 1 mM EDTA, 1% Triton X-100, 0.2 mM phenylmethylsulfonyl fluoride (PMSF), and 1× Protease Inhibitor Cocktail (P9599, Sigma-Aldrich). After centrifugation at 4,000×g at 4℃ for 5 min, the supernatant was subsequently centrifugated at 20,000×g at 4℃ for 15 min and the resulting supernatant was collected. A 25–750 µg of the crude extract was incubated with 5 µl Streptavidin-agarose (S1638, Sigma-Aldrich) at 4℃ overnight under 5 rpm end-to-end rotation. The beads collected by centrifugation at 2,500×g and 4 ℃ for 5 min were washed with a lysis buffer containing 0.1% Triton X-100 once. After centrifugation at 2,500×g at 4`℃ for 5 min, the beads were eluted with 2× SDS sample buffer containing 100 mM Tris-HCl (pH 6.8), 20% glycerol, 4% SDS, and 100 mM dithiothreitol (DTT) with additional 0.4 M urea.

Co-immunoprecipitation assay

The 11-day-old Col-0, *UBQ10:*GFP, and *UBQ10:At*SAR1c-GFP seedlings (Zeng et al., 2015) were grown with 7 days of Pi starvation. The roots were harvested for total protein extraction with lysis buffer containing 25 mM HEPES (pH 7.2), 150 mM NaCl, 0.5% IGEPAL CA-630 (I8896, Sigma-Aldrich), 2 mM EDTA, 0.5 mM $MgCl_2$ and 1× Protease Inhibitor Cocktail (P9599, Sigma-Aldrich). The supernatants were obtained by centrifugation at 16,000×g at 4℃ for 5 min and incubated with 2.5 mM dithiobis [succinimidyl propionate] (DSP) at RT for 30 min. Unreacted DSP was quenched with 100 mM Tris (pH 7.4) at RT for 15 min. A 15–750 µg of protein mixture was incubated with 5 µl of GFP-Trap® Agarose (ChromoTek) at 4℃ for 2

h with end-over-end rotation at 5 rpm, washed with the lysis buffer once, centrifuged at 2,500×g at 4℃ for 5 min, and eluted with 2× SDS sample buffer containing 100 mM Tris-HCl (pH 6.8), 20% glycerol, 4% SDS, and 100 mM DTT.

Immunoblot analysis

Protein samples were loaded onto 4–12% Q-PAGE™ Bis-Tris Precast Gel (SMOBIO) and transferred to polyvinylidene difluoride (PVDF) membranes (IPVH00010 Immobilon-P Membrane, Merck). The membrane was blocked with 1% BSA in 1× PBS solution containing 0.2% Tween 20 (PBST, pH 7.2) at RT for 1 h and hybridized with primary antibodies: anti-*At*PHF1 (Huang et al., 2013) at RT for 2 h, anti-PIP2;7 (1:5,000, AS22 4812, Agrisera), anti-mCherry (1:1,000, ab167453, Abcam), and anti-S11 (1:10,000) at RT for 1 h, the anti-S11 polyclonal rabbit antibody was raised against the peptide of S11 (EKRDHMVLLEYVTAAGITDASC) and produced by LTK BioLaboratories, Taiwan. The membrane was washed four times with 1× PBST for 5 min, followed by hybridization with the horseradish peroxidase-conjugated secondary antibody (1:20,000–1:40,000, GeneTex) in blocking solution at RT for 1 h. After four washes in 1× PBST for 5 min and a rinse with distilled water, chemiluminescent substrates (WesternBrightTM ECL and WesternBrightTM Sirius, Advansta) for signal detection were applied.

Chemical treatment

Acetosyringone (150 mM stock in DMSO, D134406, Sigma-Aldrich) was diluted to a final concentration of 150 μM in ddH_2O. β-estradiol (36.5 mM stock in DMSO, E2758, Sigma-Aldrich) was diluted to a final concentration of 9.18 μM in ddH_2O. Dithiobis [succinimidyl propionate] (25 mM stock in DMSO, 22586, ThermoFisher) was diluted to a final concentration of 2.5 mM in ddH_2O.

Accession Numbers

Sequence data from this article can be found in the Arabidopsis Genome Initiative under the following accession numbers: *At*PHF1 (At3g52190), *At*SEC12 (At2g01470), *At*PHT1;1 (At5g43350), *At*SAR1b (At1g56330), *At*SAR1c (At4g02080), *At*SEC24a (At3g07100), *At*SEC13a (At3g01340), *At*SEC16a (At5g47480).

Supplementary Data

Supplementary Figure S1. Expression of *AtSAR1* isoforms in Col-0 under Pi deprivation by RNA-seq analysis. Expression of *AtSAR1a/b/c/d/e* in the shoot and root of 10-day-old WT (Col-0) seedlings under Pi-sufficient conditions (+P0) or under one day (–P1) and three days of Pi starvation (–P3) as previously described (Liu et al., 2016). RPKM stands for reads per kilobase of transcript per million mapped reads. Numbers represent average RPKM values of two replicates, with an assigned value of 0.25 for readings below this threshold.

Supplementary Figure S2. *At*PHT1;1-induced *At*PHF1 puncta co-localize with *At*SAR1c in agro-infiltrated *N. benthamiana* leaves. (A) Expression and distribution of *At*SAR1b-S11, *At*SAR1c-S11, and *At*SEC24a-S11. The confocal images were taken at the peripheral layer of epidermal cells. Scale bars, 5 μm. (B) Co-expression of *At*PHT1;1, *At*PHF1-mCherry, and cytosolic GFP1–10 with *At*SAR1c-S11. Arrows indicate the punctate structures labeled by *At*PHF1-mCherry correspond to those labeled by the ERES marker. The puncta not overlapped are circled. Scale bars, 5 μm. (C) Distribution of the Pearson's correlation coefficient between *At*PHF1-mCherry and GFP signals of the ERES markers. The number of punctate structures used for the quantification analysis is shown in the parentheses. Data were collected from three independent experiments. For the box plot, center lines show the medians; box limits indicate the 25th and 75th percentiles; whiskers extend to minimum and maximum values; crosses represent means. Data used for quantification analysis of *At*SAR1b is the same as in **Fig. 2C**.

Supplementary Figure S3. Subcellular distribution of truncated *At*PHF1 variants in agro-infiltrated *N. benthamiana* leaves. (A and B) The expression and distribution of the S10-tagged truncated *At*PHF1 variants (A) and the S11-tagged truncated *At*PHF1 variants (B). Scale bars, 20 μm.

Supplementary Figure S4. Detection of *At*SAR1b/[H74L]/[T34N] in the soluble and microsomal fractions. Protein expression of *At*SAR1b/[H74L]/[T34N]-S11 in the agro-infiltrated tobacco leaves. The soluble (S) and microsomal (M) fractions were isolated by the low-speed pellet (LSP) method, as previously reported (Yoshimoto et al., 2004). Anti-S11 antibody was used to detect S11 fusion proteins. The membrane association was calculated as a percentage of the intensity of the M fraction by the sum of the S and M fractions. Detection of the plasma membrane aquaporin PIP2;7 was used as microsomal fraction control. Amido black staining was used as loading control.

Supplementary Table S1. Oligonucleotides used for plasmid constructs.

Funding

This work was supported by the Ministry of Science and Technology (MOST 108-2311-B-007-003-MY3) and the National Science and Technology Council (NSTC 112-2313-B-007-001-MY3).

Acknowledgments

We thank Dr. Liwen Jiang at the Chinese University of Hong Kong, People's Republic of China, for sharing the *Arabidopsis* seeds of *UBQ10:At*SAR1c-GFP and *UBQ10:*GFP homozygous lines, Dr. Masaki Takeuchi at the University of Tokyo, Japan, for sharing the clone

*35S:At*SAR1b[H74L], and Dr. Tzyy-Jen Chiou at Academia Sinica, Taiwan (R.O.C.), for sharing the clone *35S:At*PHF1-mCherry. We acknowledge Ms. Wen-Chun Chou for constructing the plasmid encoding *35S:*GFP1–10 and the technical support from the confocal image core, National Tsing Hua University (sponsored by MOST 108-2731-M-007-001, and MOST 110-2731-M-007-001).

Author Contributions

T.-Y. L. conceived the original research plan, designed and supervised the experiments and wrote the article. H.-F. L. designed and performed the experiments, analyzed the data, wrote the article and contributed to the figure preparation. J.-D. C. designed and performed the experiments.

Disclosures

The authors have no conflicts of interest to declare.

Figure Legends

Figure 1. *At*PHT1;1 overexpression triggers partial distribution of *At*PHF1 to the punctate structures in agro-infiltrated *N. benthamiana* leaves. (A) Distribution of *At*PHF1-GFP in the absence or presence of the co-expression of *At*PHT1;1-S11 or *At*STP1-S11. Arrows indicate punctate structures. Scale bars, 5 μm. (B) Quantification of *At*PHF1-GFP-labeled punctate structures. Images were collected from 4–5 independent experiments. The number of regions of interest (ROI) used for quantification is shown in parentheses. For the box plot, center lines show the medians; box limits indicate the 25th and 75th percentiles; whiskers extend to the 5th and 95th percentiles; data points are plotted as dots. Data significantly different from the *At*PHF1-GFP expression alone are indicated (*** $P < 0.001$; Student's *t*-test, two-tail).

Figure 2. *At*PHT1;1-induced *At*PHF1 puncta partially co-localizes with the ERES markers in agro-infiltrated *N. benthamiana* leaves. (A and B) Co-localization of *At*SAR1b-S11 (A) and *At*SEC24a-S11 (B) with *At*PHF1-mCherry in the absence or presence of *At*PHT1;1 overexpression. Images were taken at the peripheral layer of the epidermis. Arrows indicate the co-localization of punctate structures between the *At*PHF1-mCherry and the ERES markers. The non-overlapping puncta are circled. Scale bars, 5 μm. (C) Distribution of the Pearson's correlation coefficient between *At*PHF1-mCherry and GFP signals of the ERES markers. The number of punctate structures used for the quantification analysis is shown in the parentheses. Data were collected from three independent experiments. For the box plot, center lines show the medians; box limits indicate the 25th and 75th percentiles; whiskers extend to minimum and maximum values; crosses represent means. Data significantly different from the *At*SAR1b are indicated (*** $P < 0.001$; Student's *t*-test, two-tail).

Figure 3. *At*PHF1 interacts with *At*SAR1b and *At*SAR1c *in planta* based on the tripartite split-GFP assay in agro-infiltrated *N. benthamiana* leaves. (A) The expression and distribution of S10-*At*SEC12, S10-*At*PHF1, and the COPII-related components *At*SAR1b-, *At*SAR1c-, *At*SEC24a-, *At*SEC16a-, and *At*SEC13a-S11. Scale bars, 10 μm. (B) The interaction of S10-*At*SEC12 or S10-*At*PHF1 with the COPII-related components *At*SAR1b-, *At*SAR1c-, *At*SEC24a-, *At*SEC16a-, and *At*SEC13a-S11. Scale bars, 5 μm.

Figure 4. *At*PHF1 interacts with *At*SAR1b *in planta* based on the proximity labeling in agro-infiltrated *N. benthamiana* leaves. (A) Schematic diagrams of mTb-fused bait protein in the proximity of prey protein. The reactive intermediate biotinyl- 5'-AMP biotinylates proximal prey proteins. The grey region indicates the distance range of biotinylation. (B) The expression and subcellular distribution of mTb-NES-EYFP and *At*SAR1b-mTb-S11. Scale bars, 20 μm. (C) The interaction analysis of *At*PHF1-mCherry and *At*SAR1b by proximity labeling. Co-

expression of mTb-NES-EYFP or *At*SAR1b-mTb-S11 with *At*SEC12-mCherry or *At*PHF1-mCherry. Anti-S11 antibody was used to detect EYFP-tagged and S11-tagged fusion proteins.

Figure 5. Co-immunoprecipitation of *At*SAR1c-GFP with the endogenous *At*PHF1 and *At*PHT1;1/2/3 in *Arabidopsis* transgenic plants. (A and B) The interaction analyses of *At*SAR1c-GFP with the endogenous *At*PHF1 and *At*PHT1;1/2/3 in 11-day-old wild-type (Col-0), *UBQ10:*GFP, and *UBQ10:At*SAR1c-GFP seedlings subjected to Pi deprivation (0 μM KH_2PO_4, 7 days of starvation). The protein amounts used for input and IP in (A) and (B) were shown as indicated. Anti-S11 antibody was used to detect GFP fusion proteins.

Figure 6. *At*SAR1b and *At*SAR1c interact with the cytosolic and transmembrane domains of *At*PHF1 in agro-infiltrated *N. benthamiana* leaves. (A) Schematic diagram of the truncated *At*PHF1 variants. Domain boundaries are indicated by amino acid numbers. (B and C) The interaction analyses of the S10-*At*PHF1 truncated variants and *At*SAR1b-S11 (B) or *At*SAR1c-S11 (C). Scale bars, 10 μm.

Figure 7. *At*PHF1 preferentially interacts with the GDP-locked inactive form of *At*SAR1b in agro-infiltrated *N. benthamiana* leaves. (A) The expression and distribution of *At*SAR1b/[H74L]/[T34N]-S11. (B) The interaction analyses of S10-*At*SEC12 or S10-*At*PHF1 with *At*SAR1b/[H74L]/[T34N]-S11. Chlorophyll autofluorescence was used as a chloroplast marker. Scale bars, 5 μm.

Figure 8. Hypothetical model depicting a role for *At*PHF1 in COPII recruitment for the ER export of *At*PHT1 proteins. The GEF SEC12 recruits and activates SAR1 GTPase by exchanging of GDP to GTP. The direct interaction of GTP-bound SAR1 with SEC23 recruits SEC23/24 to form the inner coat, followed by SEC13/31 recruitment to form the outer coat.

The ER-resident PHF1 concentrates on ERES triggered by increased PHT1 proteins and interacts with GDP-bound SAR1. While the scaffold protein SEC16 at ERES does not interact with PHF1, the interaction of PHF1 and SAR1 may link to the regulation of SAR1 GTPase cycle, thereby accelerating COPII assembly at ERES to facilitate the ER-to-Golgi transport of PHT1 proteins in the budding COPII vesicles.

References

Barlowe CK, Miller EA (2013) Secretory protein biogenesis and traffic in the early secretory pathway. Genetics **193:** 383-410

Bayle V, Arrighi JF, Creff A, Nespoulous C, Vialaret J, Rossignol M, Gonzalez E, Paz-Ares J, Nussaume L (2011) Arabidopsis thaliana high-affinity phosphate transporters exhibit multiple levels of posttranslational regulation. The Plant Cel **23:** 1523-1535

Bi X, Corpina, R. A., & Goldberg, J. (2002) Structure of the Sec23/24-Sar1 pre-budding complex of the COPII vesicle coat. Nature **419:** 271-277

Cabantous S, Nguyen HB, Pedelacq JD, Koraichi F, Chaudhary A, Ganguly K, Lockard MA, Favre G, Terwilliger TC, Waldo GS (2013) A new protein-protein interaction sensor based on tripartite split-GFP association. Scientific reports **3:** 2854

Chiu C-Y, Tsai C-D, Wang J-Y, Tsai M-H, McGinness AJ, Lung H-F, Kanno S, Kriechbaumer V, Liu T-Y (2024) Phosphate starvation-induced CORNICHON HOMOLOG 5 as endoplasmic reticulum cargo receptor for PHT1 transporters in Arabidopsis. bioRxiv **06**

Chung KP, Zeng Y, Jiang L (2016) COPII paralogs in plants: functional redundancy or diversity? Trends in Plant Science **21:** 758-769

Connerly PL, Esaki M, Montegna EA, Strongin DE, Levi S, Soderholm J, Glick BS (2005) Sec16 is a determinant of transitional ER organization. Current Biolog **15:** 1439-1447

d'Enfert C, Wuestehube, L. J., Lila, T., & Schekman, R. (1991) Sec12p-dependent membrane binding of the small GTP-binding protein Sar1p promotes formation of transport vesicels from the ER. The Journal of cell biology **114:** 663-670

daSilva LL, Snapp EL, Denecke J, Lippincott-Schwartz J, Hawes C, Brandizzi F (2004) Endoplasmic reticulum export sites and Golgi bodies behave as single mobile secretory units in plant cells. The Plant Cell **16:** 1753-1771

Dharmasiri S, Swarup, R., Mockaitis, K., Dharmasiri, N., Singh, S. K., Kowalchyk, M., ... & Estelle, M. (2006) AXR4 is required for localization of the auxin influx facilitator AUX1. Science **312:** 1218-1220

Gimeno RE, Espenshade, P., & Kaiser, C. A. (1995) SED4 encodes a yeast endoplasmic reticulum protein that binds Sec16p and participates in vesicle formation. The Journal of cell biology **131:** 325-338

Gonzalez E, Solano R, Rubio V, Leyva A, Paz-Ares J (2005) PHOSPHATE TRANSPORTER TRAFFIC FACILITATOR1 is a plant-specific SEC12-related protein that enables the endoplasmic reticulum exit of a high-affinity phosphate transporter in Arabidopsis. The Plant Cell **17:** 3500-3512

Hanton SL, Chatre L, Matheson LA, Rossi M, Held MA, Brandizzi F (2008) Plant Sar1 isoforms with near-identical protein sequences exhibit different localisations and effects on secretion. Plant Molecular Biology **67:** 283-294

Hanton SL, Chatre L, Renna L, Matheson LA, Brandizzi F (2007) De novo formation of plant endoplasmic reticulum export sites is membrane cargo induced and signal mediated. Plant Physiology **143:** 1640-1650

Hanton SL, Matheson LA, Chatre L, Brandizzi F (2009) Dynamic organization of COPII coat proteins at endoplasmic reticulum export sites in plant cells. The Plant Journal **57:** 963-974

Huang TK, Han CL, Lin SI, Chen YJ, Tsai YC, Chen YR, Chen JW, Lin WY, Chen PM, Liu TY, Chen YS, Sun CM, Chiou TJ (2013) Identification of downstream components of ubiquitin-conjugating enzyme PHOSPHATE2 by quantitative membrane proteomics in Arabidopsis roots. The Plant Cell **25:** 4044-4060

Joiner AMN, Fromme JC (2021) Structural basis for the initiation of COPII vesicle biogenesis. Structure **29:** 859-872 e856

Kodera C, Yorimitsu T, Nakano A, Sato K (2011) Sed4p stimulates Sar1p GTP hydrolysis and promotes limited coat disassembly. Traffic **12:** 591-599

Kota J, Ljungdahl PO (2005) Specialized membrane-localized chaperones prevent aggregation of polytopic proteins in the ER. The Journal of cell biology **168:** 79-88

Kurokawa K, Nakano A (2019) The ER exit sites are specialized ER zones for the transport of cargo proteins from the ER to the Golgi apparatus. The journal of biochemistry **165:** 109-114

Lau WTW, Howson, R. W., Malkus, P., Schekman, R., & O'Shea, E. K. (2000) Pho86p, an endoplasmic reticulum (ER) resident protein in Saccharomyces cerevisiae, is required for ER exit of the high-affinity phosphate transporter Pho84p. Proceedings of the National Academy of Sciences **97:** 1107-1112

Li B, Zeng Y, Jiang L (2022) COPII vesicles in plant autophagy and endomembrane trafficking. FEBS letters **596:** 2314-2323

Li B, Zeng, Y., Cao, W., Zhang, W., Cheng, L., Yin, H., ... & Jiang, L. (2021) A distinct giant coat protein complex II vesicle population in Arabidopsis thaliana. Nature Plants **7:** 1335-1346

Liang X, Li SW, Gong LM, Li S, Zhang Y (2020) COPII components Sar1b and Sar1c play distinct yet interchangeable roles in pollen development. Plant Physiology **183:** 974-985

Liu T-Y, Tsai M-H, Wang J-Y, Lung H-F, Chow H-X, Chiu C-Y, Lu C-A (2024) CORNICHON HOMOLOG 5-dependent ER export of membrane cargoes in phosphate-starved Arabidopsis root as revealed by membrane proteomic analysis. bioRxiv **12**

Liu TY, Chou WC, Chen WY, Chu CY, Dai CY, Wu PY (2018) Detection of membrane protein-protein interaction in planta based on dual-intein-coupled tripartite split-GFP association. The Plant Journal **94:** 426-438

Liu TY, Huang TK, Yang SY, Hong YT, Huang SM, Wang FN, Chiang SF, Tsai SY, Lu WC, Chiou TJ (2016) Identification of plant vacuolar transporters mediating phosphate storage. Nature communications **7:** 11095

Mair A, Xu SL, Branon TC, Ting AY, Bergmann DC (2019) Proximity labeling of protein complexes and cell-type-specific organellar proteomes in Arabidopsis enabled by TurboID. elife **8**

McMahon C, Studer SM, Clendinen C, Dann GP, Jeffrey PD, Hughson FM (2012) The structure of Sec12 implicates potassium ion coordination in Sar1 activation. Journal of Biological Chemistry **287:** 43599-43606

Miller E, Antonny, B., Hamamoto, S., & Schekman, R. (2002) Cargo selection into COPII vesicles is driven by the Sec24p subunit. The EMBO journal**:** 6105-6113

Nussaume L, Kanno S, Javot H, Marin E, Pochon N, Ayadi A, Nakanishi TM, Thibaud MC (2011) Phosphate import in plants: focus on the PHT1 transporters. Frontiers in plant science **2:** 83

Paul S, Audhya A, Cui Q (2023) Molecular mechanism of GTP binding-and dimerization-induced enhancement of Sar1-mediated membrane remodeling. Proceedings of the National Academy of Sciences **120:** e2212513120

Saito-Nakano Y, Nakano A (2000) Sed4p functions as a positive regulator of Sar1p probably through inhibition of the GTPase activation by Sec23p. Genes to Cells **5:** 1039-1048

Saito K, Yamashiro K, Shimazu N, Tanabe T, Kontani K, Katada T (2014) Concentration of Sec12 at ER exit sites via interaction with cTAGE5 is required for collagen export. Journal of Cell Biology **206:** 751-762

Schneider CA, Rasband WS, Eliceiri KW (2012) NIH Image to ImageJ: 25 years of image analysis. Nature methods **9:** 671-675

Shen J, Yuan, L., Zhang, J., Li, H., Bai, Z., Chen, X., ... & Zhang, F. (2011) Phosphorus dynamics: from soil to plant. Plant physiology **156:** 997-1005

Spitzer M, Wildenhain J, Rappsilber J, Tyers M (2014) BoxPlotR: a web tool for generation of box plots. Nature methods **11:** 121-122

Stagg SM, Gurkan C, Fowler DM, LaPointe P, Foss TR, Potter CS, Carragher B, Balch WE (2006) Structure of the Sec13/31 COPII coat cage. Nature **439:** 234-238

Supek F, Madden DT, Hamamoto S, Orci L, Schekman R (2002) Sec16p potentiates the action of COPII proteins to bud transport vesicles. The Journal of cell biology **158:** 1029-1038

Takagi J, Renna L, Takahashi H, Koumoto Y, Tamura K, Stefano G, Fukao Y, Kondo M, Nishimura M, Shimada T, Brandizzi F, Hara-Nishimura I (2013) MAIGO5 functions in protein export from Golgi-associated endoplasmic reticulum exit sites in Arabidopsis. The Plant Cell **25:** 4658-4675

Tidy A, Abu Bakar N, Carrier D, Kerr ID, Hodgman C, Bennett MJ, Swarup R (2024) Mechanistic insight into the role of AUXIN RESISTANCE4 in trafficking of AUXIN1 and LIKE AUX1-2. Plant Physiology **194:** 422-433

Van der Verren SE, Zanetti G (2023) The small GTPase Sar1, control centre of COPII trafficking. FEBS letters **597:** 865-882

Wang X, Xu M, Gao C, Zeng Y, Cui Y, Shen W, Jiang L (2020) The roles of endomembrane trafficking in plant abiotic stress responses. Journal of integrative plant biology **62:** 55-69

Wei T, Wang A (2008) Biogenesis of cytoplasmic membranous vesicles for plant potyvirus replication occurs at endoplasmic reticulum exit sites in a COPI-and COPII-dependent manner. Journal of virology **82:** 12252-12264

Weissman JT, Plutner H, Balch WE (2001) The mammalian guanine nucleotide exchange factor mSec12 is essential for activation of the Sar1 GTPase directing endoplasmic reticulum export. Traffic **2:** 465-475

Xu SL, Shrestha R, Karunadasa SS, Xie PQ (2023) Proximity labeling in plants. Annual review of plant biology **74:** 285-312

Yoshimoto K, Hanaoka H, Sato S, Kato T, Tabata S, Noda T, Ohsumi Y (2004) Processing of ATG8s, ubiquitin-like proteins, and their deconjugation by ATG4s are essential for plant autophagy. The Plant Cell **16:** 2967-2983

Zeng Y, Chung KP, Li B, Lai CM, Lam SK, Wang X, Cui Y, Gao C, Luo M, Wong KB, Schekman R, Jiang L (2015) Unique COPII component AtSar1a/AtSec23a pair is required for the distinct function of protein ER export in Arabidopsis thaliana. Proceedings of the National Academy of Sciences **112:** 14360-14365

Zhang Z, Nakamura S, Yamasaki A, Uehara M, Takemura S, Tsuchida K, Kamiya T, Shigenobu S, Yamaguchi K, Fujiwara T, Ishiguro S, Takano J (2024) Arabidopsis KNS3 and its two homologs mediate endoplasmic reticulum-to-plasma membrane traffic of boric acid channels. Journal of Experimental Botany **75:** 7046-7065

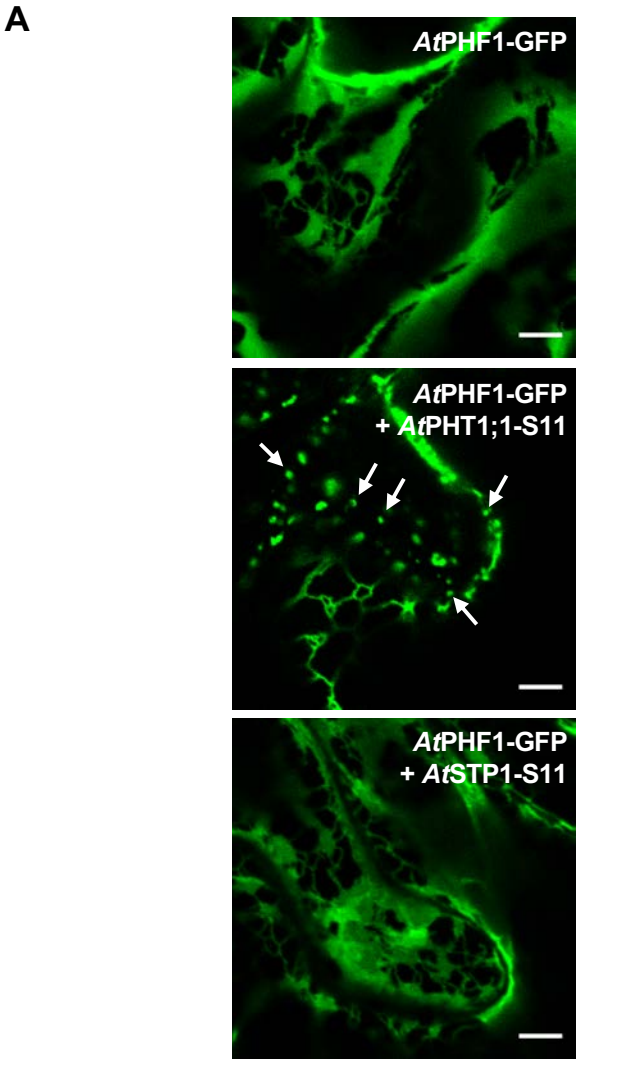

Figure 1. *At*PHT1;1 overexpression triggers partial distribution of *At*PHF1 to the punctate structures in agro-infiltrated *N. benthamiana* leaves. (A) Distribution of *At*PHF1-GFP in the absence or presence of the co-expression of *At*PHT1;1-S11 or *At*STP1-S11. Arrows indicate punctate structures. Scale bars, 5 µm. (B) Quantification of *At*PHF1-GFP-labeled punctate structures. Images were collected from 4–5 independent experiments. The number of regions of interest (ROI) used for quantification is shown in parentheses. For the box plot, center lines show the medians; box limits indicate the 25th and 75th percentiles; whiskers extend to the 5th and 95th percentiles; data points are plotted as dots. Data significantly different from the *At*PHF1-GFP expression alone are indicated (*** $P < 0.001$; Student's t-test, two-tail).

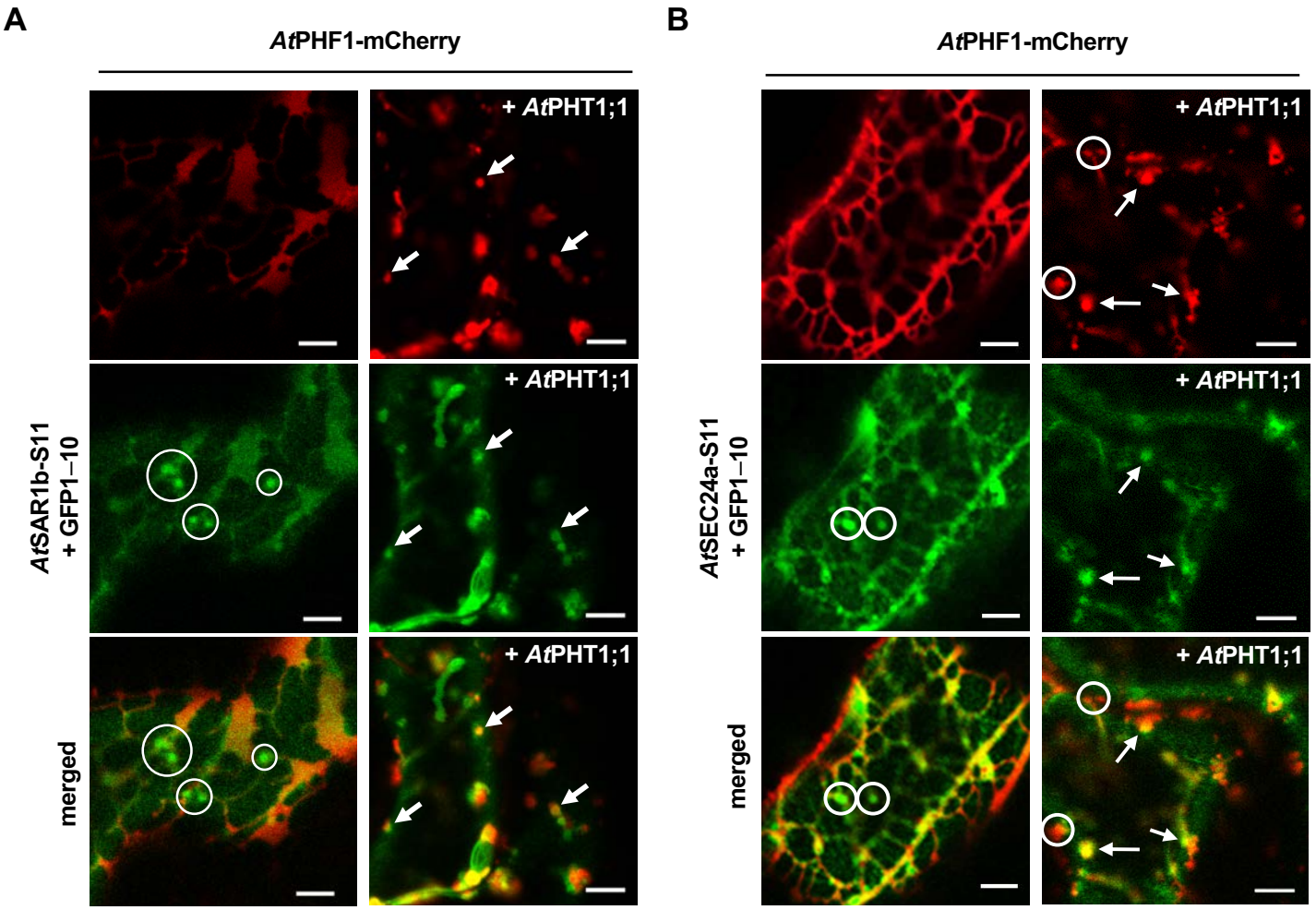

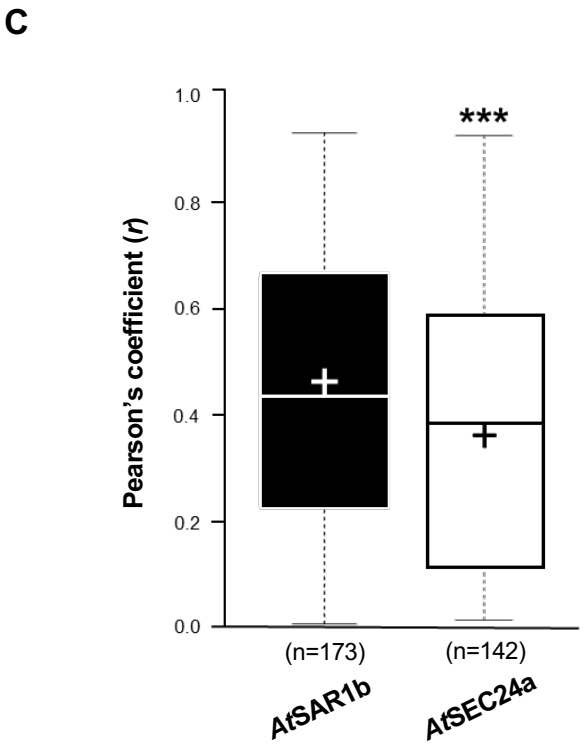

Figure 2. *At*PHT1;1-induced *At*PHF1 puncta partially colocalizes with the ERES markers in agro-infiltrated *N. benthamiana* leaves. (A and B) Co-localization of *At*SAR1b-S11 (A) and *At*SEC24a-S11 (B) with *At*PHF1-mCherry in the absence or presence of *At*PHT1;1 overexpression. Images were taken at the peripheral layer of the epidermis. Arrows indicate the colocalization of punctate structures between the *At*PHF1-mCherry and the ERES markers. The non-overlapping puncta are circled. Scale bars, 5 μm. (C) Distribution of the Pearson's correlation coefficient between *At*PHF1-mCherry and GFP signals of ERES markers. The number of punctate structures used for the quantification analysis is shown in the parentheses. Data were collected from three independent experiments. For the box plot, center lines show the medians; box limits indicate the 25th and 75th percentiles; whiskers extend to minimum and maximum values; crosses represent means. Data significantly different from the *At*SAR1b are indicated (*** $P < 0.001$; Student's *t*-test, two-tail).

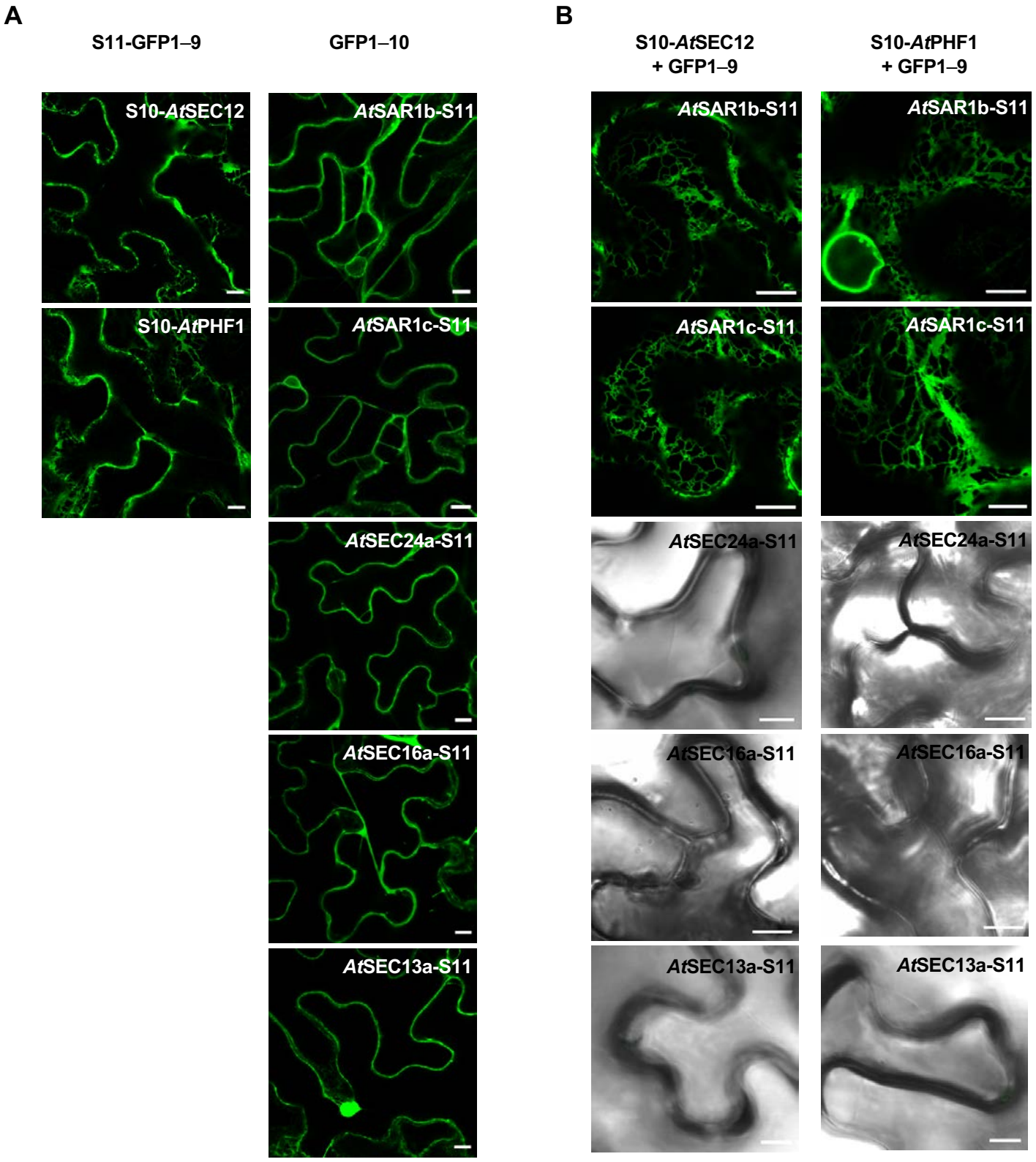

Figure 3. *At*PHF1 interacts with *At*SAR1b and *At*SAR1c *in planta* based on the tripartite split-GFP assay in agro-infiltrated *N. benthamiana* leaves. (A) The expression and distribution of S10-*At*SEC12, S10-*At*PHF1, and the COPII-related components *At*SAR1b-, *At*SAR1c-, *At*SEC24a-, *At*SEC16a-, and *At*SEC13a-S11. Scale bars, 10 μm. (B) The interaction of S10-*At*SEC12 or S10-*At*PHF1 with the COPII-related components *At*SAR1b-, *At*SAR1c-, *At*SEC24a-, *At*SEC16a-, and *At*SEC13a-S11. Scale bars, 5 μm.

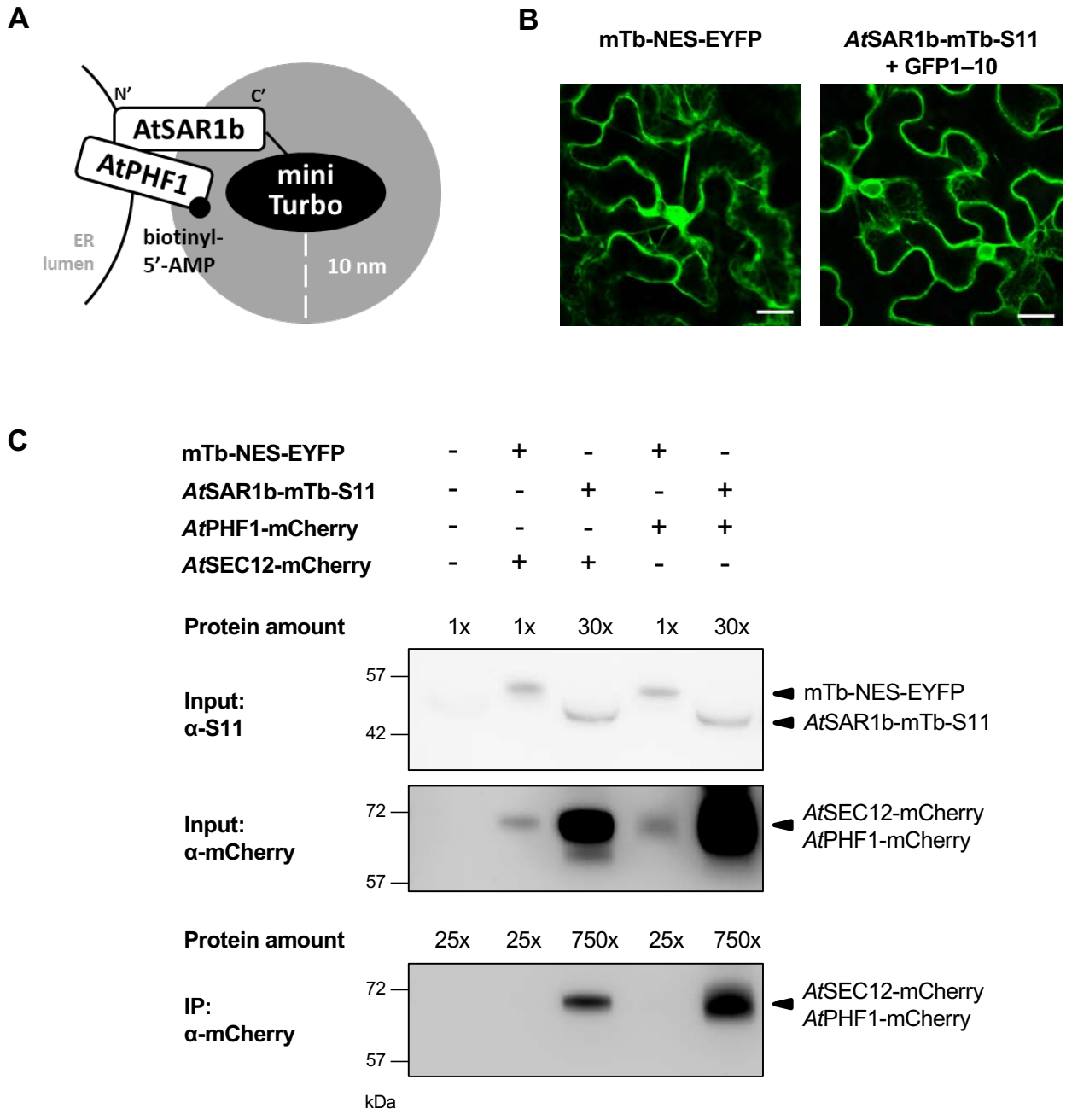

Figure 4. *At*PHF1 interacts with *At*SAR1b *in planta* based on the proximity labeling in agro-infiltrated *N. benthamiana* leaves. (A) Schematic diagrams of mTb-fused bait protein in the proximity of prey protein. The reactive intermediate biotinyl- 5'-AMP biotinylates proximal prey proteins. The grey region indicates the distance range of biotinylation. (B) The expression and subcellular distribution of mTb-NES-EYFP and *At*SAR1b-mTb-S11. Scale bars, 20 μm. (C) The interaction analysis of *At*PHF1-mCherry and *At*SAR1b by proximity labeling. Co-expression of mTb-NES-EYFP or *At*SAR1b-mTb-S11 with *At*SEC12-mCherry or *At*PHF1-mCherry. Anti-S11 antibody was used to detect EYFP-tagged and S11-tagged fusion proteins.

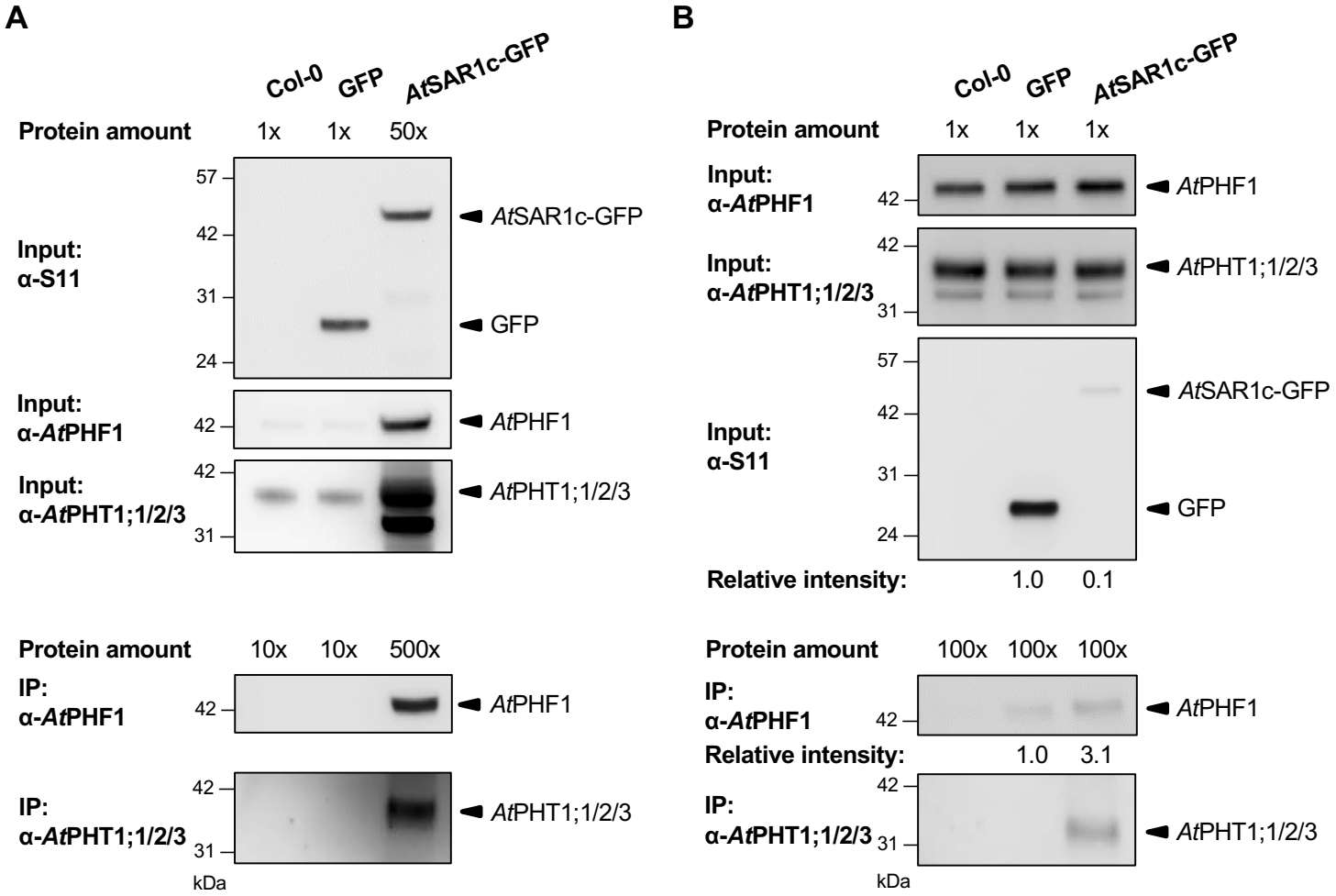

Figure 5. Co-immunoprecipitation of *At*SAR1c-GFP with the endogenous *At*PHF1 and *At*PHT1;1/2/3 in *Arabidopsis* transgenic plants. (A and B) The interaction analyses of *At*SAR1c-GFP with the endogenous *At*PHF1 and *At*PHT1;1/2/3 in 11-day-old wild-type (Col-0), *UBQ10:*GFP, and *UBQ10:At*SAR1c-GFP seedlings subjected to Pi deprivation (0 μM KH_2PO_4, 7 days of starvation). The protein amounts used for input and IP in (A) and (B) were shown as indicated. Anti-S11 antibody was used to detect GFP fusion proteins.

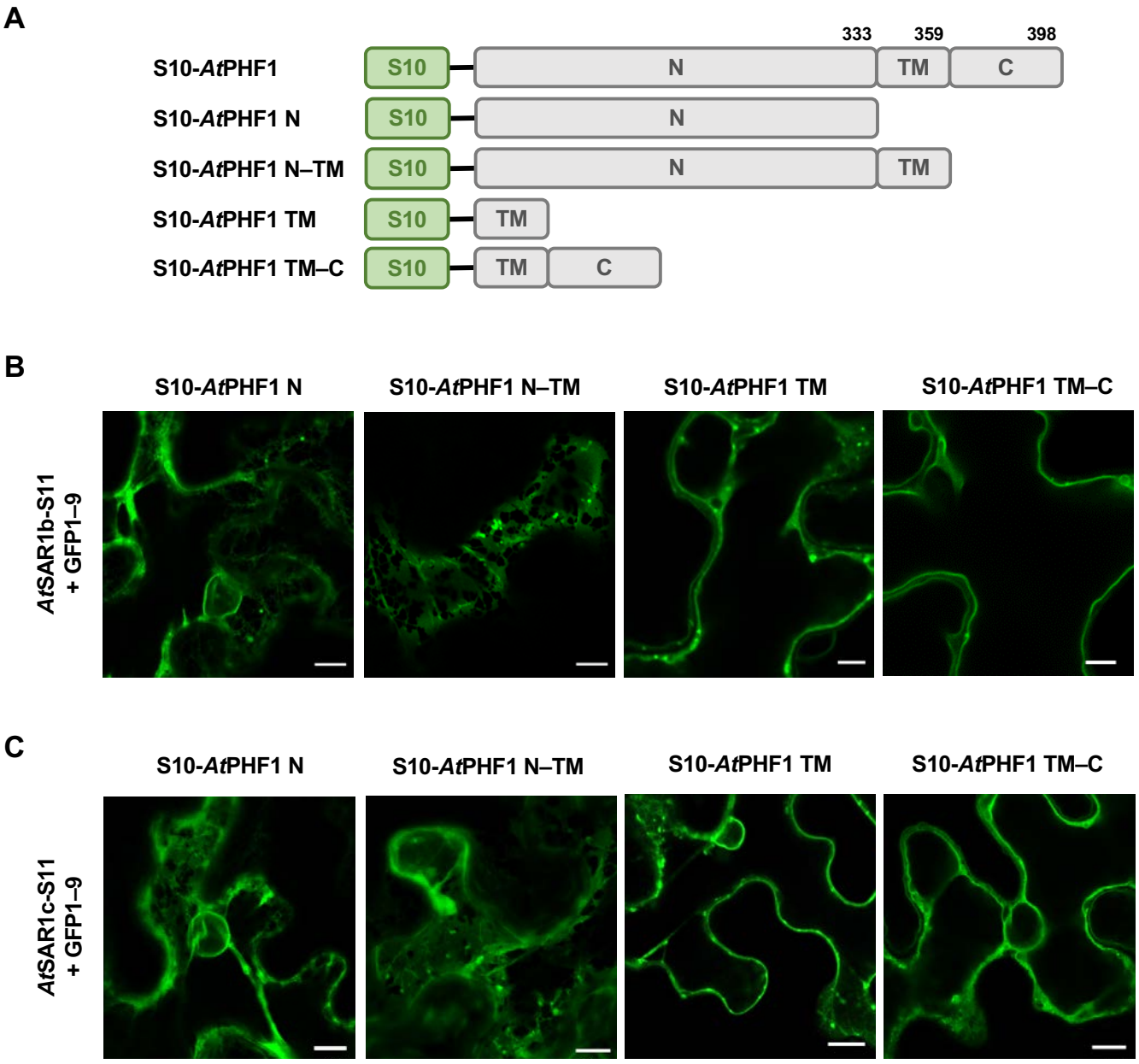

Figure 6. *At*SAR1b and *At*SAR1c interact with the cytosolic and transmembrane domains of *At*PHF1 in agro-infiltrated *N. benthamiana* leaves. (A) Schematic diagram of the truncated *At*PHF1 variants. Domain boundaries are indicated by amino acid numbers. (B and C) The interaction analyses of the S10-*At*PHF1 truncated variants and *At*SAR1b-S11 (B) or *At*SAR1c-S11 (C). Scale bars, 10 μm.

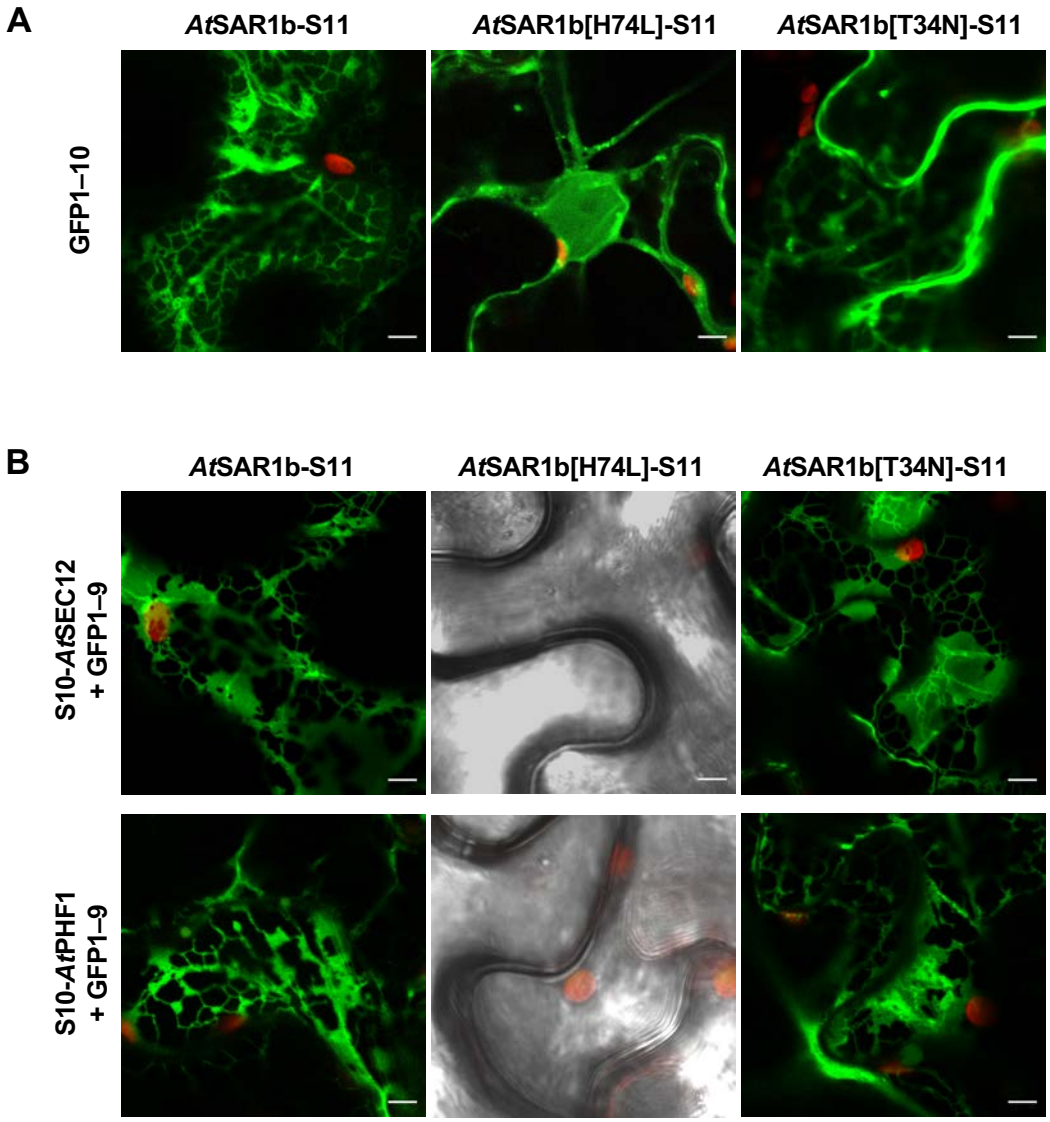

Figure 7. *At*PHF1 preferentially interacts with the GDP-locked inactive form of *At*SAR1b in agro-infiltrated *N. benthamiana* leaves. (A) The expression and distribution of *At*SAR1b/[H74L]/[T34N]-S11. (B) The interaction analyses of S10-*At*SEC12 or S10-*At*PHF1 with *At*SAR1b/[H74L]/[T34N]-S11. Chlorophyll autofluorescence was used as a chloroplast marker. Scale bars, 5 μm.

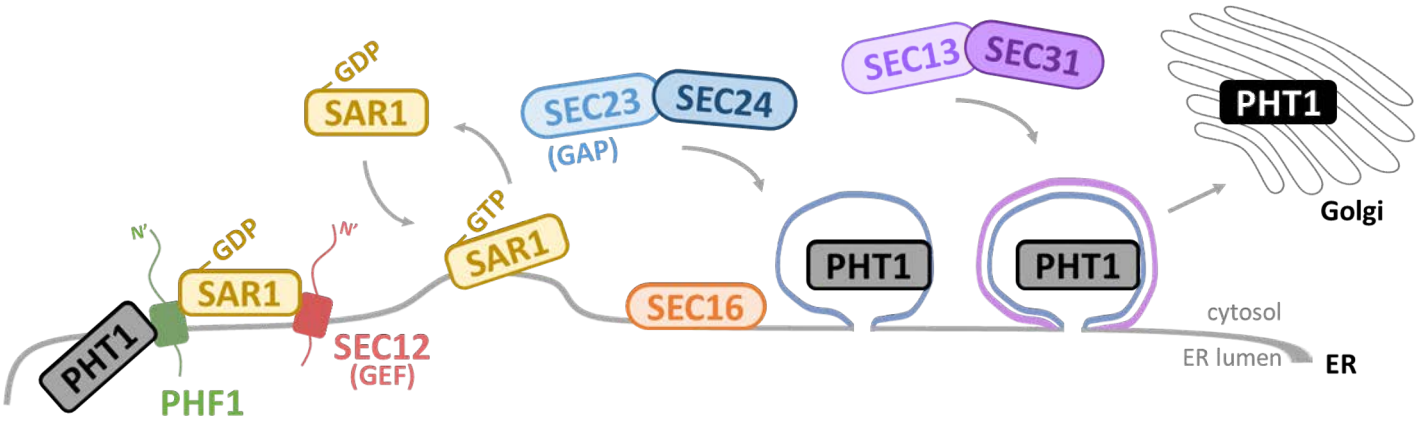

Figure 8. Hypothetical model depicting a role for *At*PHF1 in COPII recruitment for the ER export of *At*PHT1 proteins. The GEF SEC12 recruits and activates SAR1 GTPase by exchanging of GDP to GTP. The direct interaction of GTP-bound SAR1 with SEC23 recruits SEC23/24 to form the inner coat, followed by SEC13/31 recruitment to form the outer coat. The ER-resident PHF1 concentrates on ERES triggered by increased PHT1 proteins and interacts with GDP-bound SAR1. While the scaffold protein SEC16 at ERES does not interact with PHF1, the interaction of PHF1 and SAR1 may link to the regulation of SAR1 GTPase cycle, thereby accelerating COPII assembly at ERES to facilitate the ER-to-Golgi transport of PHT1 proteins in the budding COPII vesicles.